Visualization of Recirculation Zones Over a Perforated Plate: An Optical Flow Technique for Characterization of Fluid Dynamics in Structured Packing

Manasa Iyer [a], John Pachón-Morales[a], Joel Casalinho[b], Jacopo Seiwert[a], Mikael Wattiau[a], Laurent Zimmer[c], Hervé Duval[b]

[a] Air Liquide Research and Development, 1 Chemin de la Porte des Loges, Les-Loges-en-Josas 78350, France
[b] LGPM, CentraleSupélec, Université Paris-Saclay, 3 rue Joliot-Curie, 91192 Gif-sur-Yvette, France
[c] EM2C, CNRS, CentraleSupélec, Université Paris-Saclay, 3 rue Joliot-Curie, 91192 Gif-sur-Yvette, France
manasa.periyapattana@airliquide.com; laurent.zimmer@centralesupelec.fr

Abstract. The dynamics of liquid film over the perforated metallic sheets of structured packing highly influences mass transfer and pressure drop characteristics. Regarding the perforations, their role in mass transfer enhancement and liquid redistribution is yet not well understood. On perforated packing, liquid films can be either supported or suspended (‘curtain" regime, also known as "twin film"). Twin films account for intensive capillary waves and strong recirculation zones on the free surfaces. Therefore, experiments are required to assess the curtain formation in the perforations and relate it to the dynamics that intensify interfacial mass transfer.

Here, a two-dimensional two-component (2D-2C PTV) optical-flow-based technique is applied using defocused fluorescent particles images (to allow discrimination between static and dynamic particles) illuminated by a continuous laser and acquired with a high-speed camera. This provided an opportunity to evaluate the hydrodynamics of the liquid curtain through streamline patterns and to describe key features that promote mass transfer intensification within the suspended liquid curtain.

Experiments performed using an in-house test bench allowed the proposed method to be applied satisfactorily to study the behavior of a liquid film flowing over a perforated flat plate. Different recirculation regimes were observed depending on the Reynolds number: horseshoe vortices around perforations - before curtain formation, Dean vortices and kidney-pair vortices - following curtain formation. These eddies appeared chaotic for higher Reynolds numbers. Quantitatively, these recirculation zones were evidenced by negative film velocities, locally detected in the liquid curtain. In structured packing, the recirculation zones in perforations could promote mass transfer through: strong turbulent vortices favoring species transport at the interface; stagnation points with slow local liquid film velocities, increasing the local residence time, which leads to a longer gas-liquid contact time.

Keywords Structured Packing, optical flow, Liquid curtain, Perforations, Flow visualization

1 Introduction

Structured packing columns are known for large surface exchange between gas and liquid in the fluid separation process. Due to the unique design of stacking inclined corrugated and perforated metallic sheets adjacent to each other, overall surface area of the packing on which liquid films are sheared by counter-current gas flow is higher. At the same time, the dense assembly of the packing limits any access to observe and measure the nature of small-scale liquid and gas maldistribution. Only recently, a few advanced nonintrusive optical techniques such as x-ray[1], gamma-ray[2] tomography, have been implemented to see inside the packed column. Some researchers used Particle image/tracking velocimetry (PIV, PTV) on complex packing surface[3] to unravel complex flow structures in liquid film scale with high spatial resolution.

According to recent studies[4,5], liquid film on the perforated metallic sheets are of two kinds: supported liquid film and suspended liquid film, known as twin films[6] or liquid curtain[5]. Liquid film flowing on the perforation undergoes different transition mechanisms such as the rim, drop/column before forming a thin liquid curtain/sheet. The hydrodynamics of twin films are different from film on solid surfaces because they present rapid change in velocity, strong variation of thickness profiles and allows phase interaction on both faces through suspended liquid film. We expect the liquid curtain/twin film regime to be dominantly present in liquid films on corrugated and perforated elements of structured packing. The question raised here is, how appropriate is the hydrodynamics of twin liquid films, in the prospect of mass transfer, compared to the films on non-perforated elements of structured packing. How can we measure the curtain dynamics to analyze the flow structures of twin films? Therefore, further attention was given to the subject to obtain new information using new tools to quantify the complex flow structures on a simplified but relevant geometry. A flat aluminium vertical perforated sheet is considered by solely supplying with liquid on its front side.

We developed an optical set-up to conduct Particle Image Velocimetry (PIV) with a concept of defocus of tracer particles seeded to the flow, a new variation of non-intrusive optical techniques to analyze velocity components.

The method has been developed by Baudoin et al[7] and implemented to validate numerical simulation data of the mixing phenomena downstream a spacer grid in the reactor core (nuclear sector). For the first time within falling liquid films, image processing is done using optical flow algorithms[8] rather than classical Fast Fourier Transform (FFT) based PIV. The optical flow method can detect the movement of even a small change in intensity speck of light. The technique can provide a displacement vector on each pixel of the image and is thus known for its potentially high spatial resolution.

2 Description of experimental set-up

The experimental setup consists of a support system to hold the test plate in position, a hydraulic circuit including the flow distribution system to supply liquid film on both faces of the test plate. This type of supply system simulates the irrigation system used to irrigate industrial structured packings. The test plate is inserted in a rigid frame to ensure its flatness. The liquid circuit and the instrumentation are mounted on a dedicated frame. The frame holding the test plate is decoupled from the other parts of the hydraulic circuit and instrumentation. The whole assembly is mounted an anti-vibration table to damp the parasitic vibrations that may affect the fluid film flowing on the plate (see Figure 1).

The hydraulic circuit comprises of a flow loop, which is from the reservoir to the sample plate and then back to the reservoir through the liquid collector. The liquid from the reservoir circulates through the magnet gear pump (MDG-M15T3B, Iwaki) to deliver the required flow rate to the distributors on each side of the plate. Two flowmeters independently control the flow rate delivered on each face of the test plate. Needle control valves with the spillway are installed to deliver a constant and calibrated flow rate at the output.

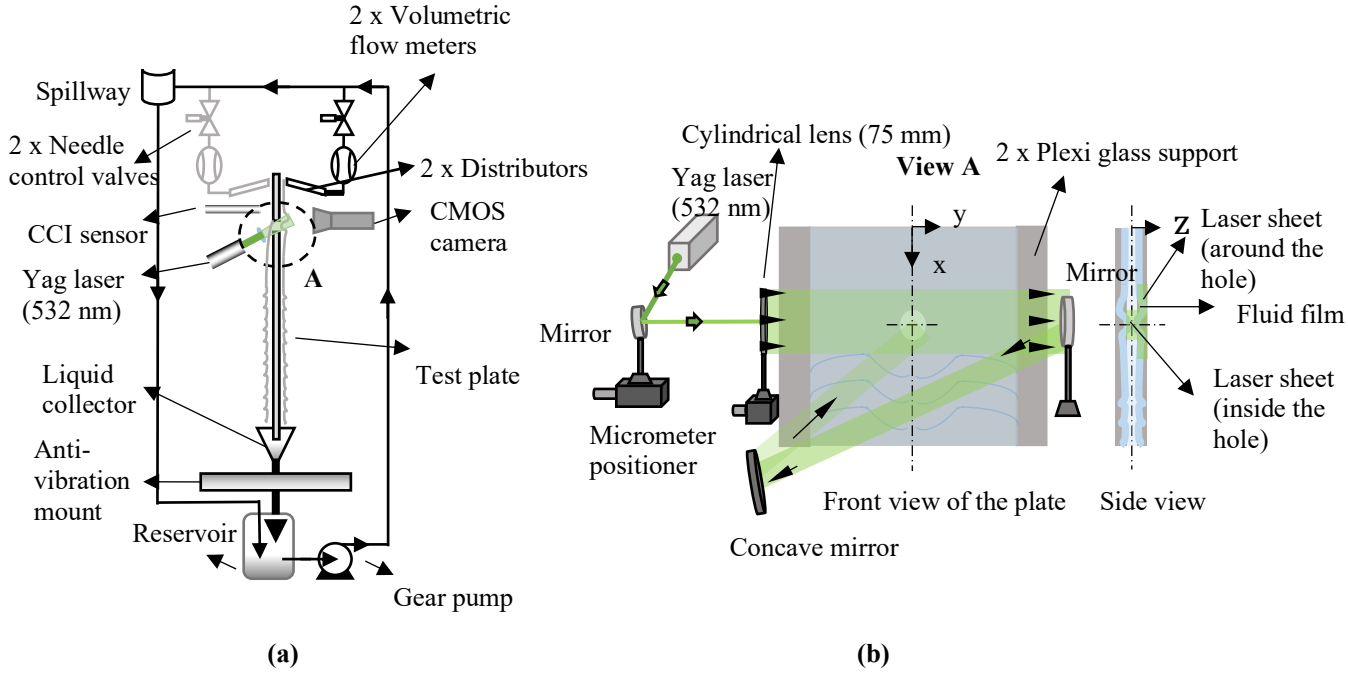


Figure 1: (a) Schematic representation of the experimental setup (one face supply configuration. (b) Light sheet optics: orientation of the laser sheet and collection optics from the front side.

Optical set-up

The optical part of the setup consists of a CMOS high-speed camera (v310, Phantom) mounted with a macro lens (AF DC-Nikkor 105 mm f/2D, Nikon), fluorescence filter (centered around 570 nm), Nd: YAG laser (532 nm - 16W - finesse Quantum), optical lens and mirrors. The continuous laser beam excites the fluorescent tracer particles seeded in the flow. The maximum output power of the laser beam is maintained up to 16 W throughout all the measurements. The laser beam is directed in the direction parallel to the falling film flow using a mirror. Then, it passes through a cylindrical lens that converts it into a laser sheet. The laser sheet is then directed over the flow from the left side to the right side (seen by the camera) on the entire width of the plate (see Figure 1). The width of the sheet in the x-direction is approximately 12 mm. The intensity is homogeneous in the zone of measurement in the plate's streamwise (x) and span-wise (y). An additional optical setup is used to visualize the hole area (specific to perforated plate). A combination of two mirrors and a convex lens with a pre-set tilt angle is used to refocus the laser beam in the hole.

All the images are captured with a resolution of 1200×800 px² at a sample rate of 800 Hz and an exposure time of 1200 µs. A fluorescence filter is used between the objective and the sensor to visualize the fluorescent tracer particles. The filter avoids capturing parasite reflections emitted by the aluminum plate, deformation on the free surface film and other reflective surfaces present around the setup. The frontal view of the plate is visualized by the camera (see Figure 1) The camera is installed on a precision positioning platform to adjust its orientation in all three dimensions precisely.

The selection criterion for the properties of the tracer particles (diameter (d_p), density (ρ_p)) is based on the Stokes number (St). This number calculates the ratio between the response time of the particles (τ_p) to the Kolmogorov time scale (τ_κ) of the flow.

$$St = \frac{\tau_p}{\tau_\kappa} \; with \; \tau_p = d_p^2 . \frac{\rho_p}{18\,\mu}$$

where ρ_p is the density of the particle, d_p is the diameter of the particle and μ is the dynamic viscosity of the liquid. $St << 1$ signifies that the particle perfectly follows the flow streamlines. Furthermore, as the aim is to track individual particles, the amount of particles in the liquid remains limited. In our experiments, the size of the particles is 20 μm.

Before each experiment, the test plate is cleaned with a surfactant solution (3 vol%, Mucasol, Merz), thoroughly rinsed with distilled water, and dried with compressed air. The parallelism of the test plate is carefully adjusted in order to obtain a liquid film of uniform thickness in the spanwise (y) direction. Both faces of the plate are supplied with the highest flow rate, i.e. 65 L.h^{-1}, such that the liquid is forced to wet fully the usable width of the plate, i.e. $W = 90$ mm. Then, the liquid flow rate can be reduced down to 5 L.h^{-1} and the region upstream of the perforation remains totally covered by the liquid film.

3 Methodology

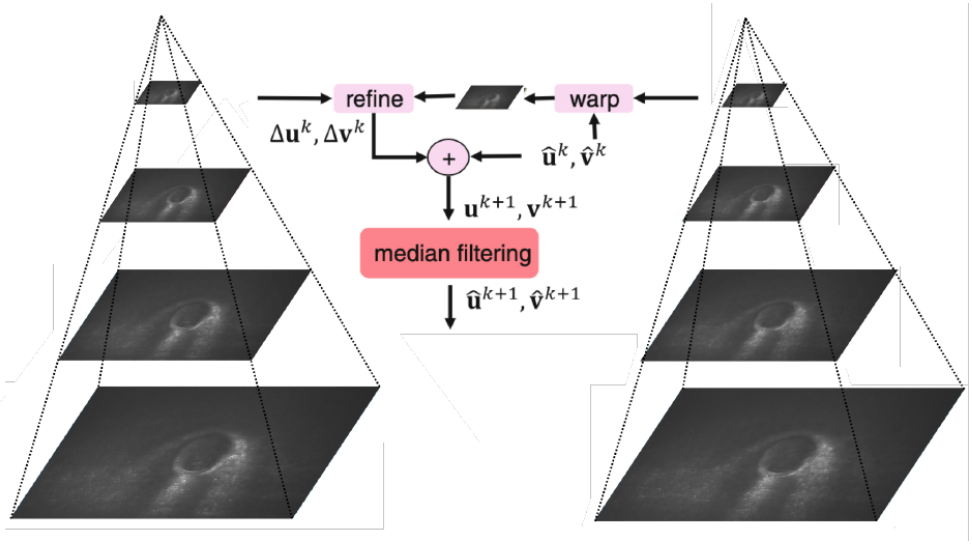


Figure 2: Optical flow algorithm

Images of the particles are processed using an optical flow algorithm approach[8]. The principle is to determine the intensity displacement (considered an invariant scalar) between two images.

$$E(\boldsymbol{u},\boldsymbol{v}) = \sum_{i,j} \Big\{ \rho_D \left(I_1(i,j) - I_2\big(i + u_{i,j}, j + v_{i,j}\big) \right) + \lambda \big[\rho_S\big(u_{i,j}, j + u_{i+1,j}\big) + \rho_S\big(u_{i,j} - u_{i,j+1}\big) + \rho_S\big(v_{i,j} - v_{i+1,j}\big) + \rho_S\big(v_{i,j} - v_{i,j+1}\big) \big] \Big\}$$

The choice of the different penalty functions leads to significant differences. These penalties are generally determined empirically: according to the actual images. A pyramidal approach is used (see Figure 2): we start from an image of shallow resolution to increase, at each level, the resolution. To assess the best approach possible, time-series data are used, and typical displacement between image at an instant t and instant $t + 1$ is added to the displacement computed between image at an instant $t + 1$ and instant $t + 2$. This result is then

compared to the displacement measured between image t and image $t+2$. This provides the most consistent processing technique, leading to the lowest uncertainties. In the present investigation, the results of a parametric investigation show that optimum parameters are the following. The penalty function $\rho(x)$ is set as the Charbonnier penalty[9] $\sqrt{x^2+\epsilon^2}$ and ϵ is set to 0.0010.

4. Results

We presently report experiments carried out with propan-2-ol at wide range of supply flowrate on one side of the plate. The liquid film in the perforation is operated in curtain mode. This particular transition is observed to be associated with profound modifications of the flow pattern on the front side and backside of the plate. The liquid curtain is also highly hysteretique, i.e. once formed curtain in the perforation is maintained even when the supply flowrate is reduced. The curtain ruptures at very low flowrates (slightly higher than zero). We expect that the hydrodynamics of liquid curtain, if manifests in an actual structured packing column, could potentially affect the interfacial mass transfer.

4.1. Visualization of recirculation zones in the suspended liquid curtain in perforation

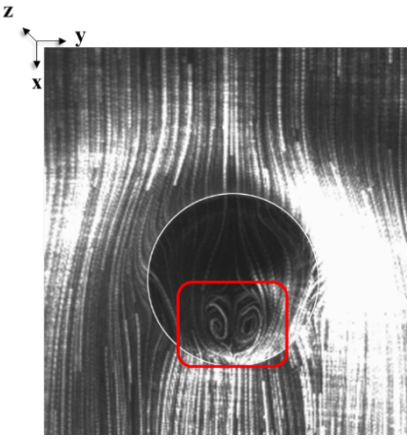


Figure 3: 20 superposed images of fluid film with florescent tracer particles showing streamlines in $x-y$ in the liquid film on a perforated plate (d = 4 mm) using propan-*2-ol* (μ = 0.002 Pa.s, σ = 0.021 N/m) (Re = 34, Ka = 348).

The flow structures in the liquid film operating in curtain mode have been examined by superposing several images of the liquid film on a perforated plate, captured at a sampling rate of 800 Hz (exposure time of 1.2 ms) (see Figure 3). The particle trajectories in the flow appears in the form streamlines Two distinctive vortices of kidney bean shape, rotating in counter clockwise direction, is observed in $x-y$ plane within the liquid curtain. The vortices are localized just above the inner surface of the perforation exit.

5. Probability density distribution of velocity vectors

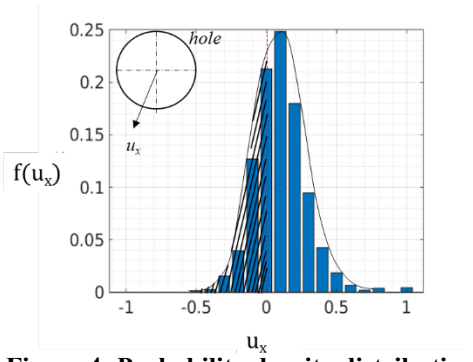


Figure 4: Probability density distribution of the axial velocity vectors at supply flow rate of 0.26 m^3/m.h^{-1} and mean theoretical velocity is u_{th}= 0.23 ms^{-1}.

In the next step, we aim to quantify the recirculation zones or vortices observed qualitatively. The probability density distribution of the measure axial velocity vectors ($\overrightarrow{u_x}$) is plotted. The probability density distribution of the time series axial velocities vectors measured at the center of the perforation are presented in figure 4. The probability distribution takes the form of normal distribution centered at the mean value of 0.1. We observe both positive and negative velocity vectors. The flow velocity is globally positive; however, the intensity of the events with negative velocities is non-negligible. These velocity vectors correspond to the particles that move in the reverse flow direction. It is to be noted that the results are presented in pixels to address the uncertainty in measured values, approximately of the order of 0.05 px.

Following the same approach, we examine the probability of negative velocity in the liquid curtain using 2D color maps (see Figure 5) in $x-y$ plane. The color scale ranges between 0 (deep blue) to 0.5 (pale yellow), corresponding to 0% occurrence of negative velocity vectors to almost 50% occurrence.

x and y coordinates are centered by considering the center of the perforation as a reference. The black lines are the steady streamlines, and they represent the mean flow path. For clarity purposes, only a few lines are drawn. We observe the strong intensity of negative velocities in the entrance, center, and exit of the perforation. This localized negative velocity region consistently increases with supply Reynolds number. In Figure 5(b), the negative velocity dominant region extends radially in the perforation, covering 60% of the liquid curtain.

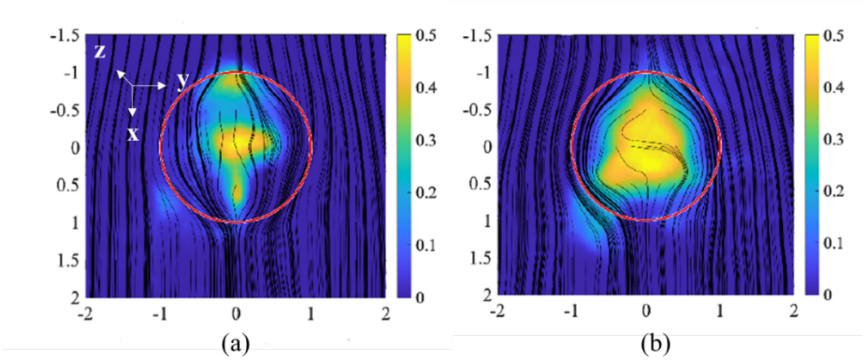


Figure 5: Probability density map of the negative velocities in and around the perforation in curtain mode for supply flow rates per unit width of the film (a) Q = 0.18 m³/m.h (b) Q = 0.47 m³/m.h. Diameter of the perforation $d = 4$ mm and plate thickness $t = 0.5$ mm. Test liquid is propan-2-ol.

3.3. Flow characteristics through DMD post processing

In order to characterize the flow dynamics in the liquid curtain, Dynamic Mode Decomposition (DMD) type of post processing method is applied. DMD is a mathematical tool widely used to extract the dynamical structures from the experimental/numerical time resolved 2D dataset. The post processing method is applied to 3000 snapshots to extract dominant frequency modes in the flow field. When examining the spectra of the DMD amplitude, one can notice a principal peak at a specific frequency, with a signal-to-noise ratio of 1.6. This frequency is identified as a dominant DMD mode. In Figure 6, a dominant frequency mode of 26 Hz is observed for a given mean axial velocity (at $u_{th} = 0.23$ ms^{-1}; Q = 0.26m³/mh). Similarly, DMD is applied for the flow fields with different mean axial velocities of the liquid film. We note that the peak frequency identified for each supply condition increases linearly ($R^2 = 0.99$) with the increase in mean axial velocity. Interestingly, the linear fit do not pass through zero when f is zero. It is probably related to a characteristic mean velocity of curtain rupture, which is slightly higher than zero.

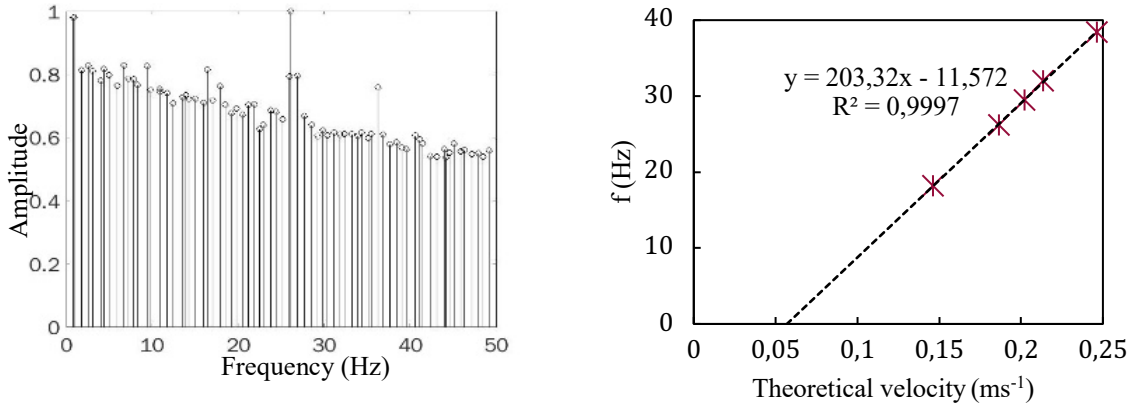
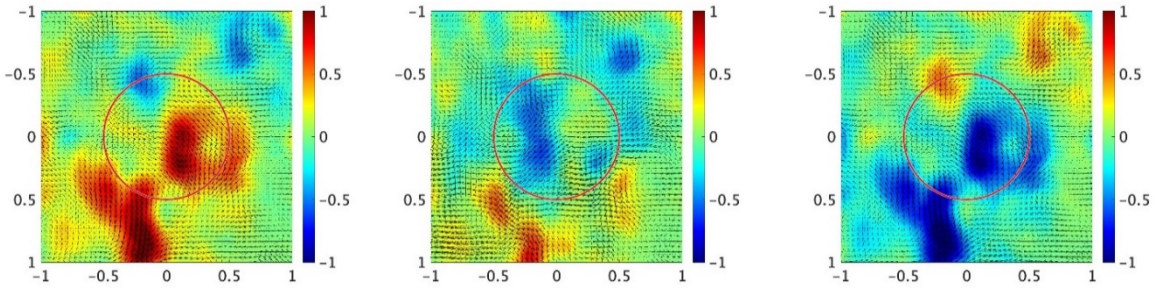


Figure 6 : Left: Oscillation frequencies obtained from DMD post processing. Right: Dominant frequency modes as a function of mean axial velocity.

In DMD, a frequency is associated with a spatial mode, and the typical streamlines associated with those modes are shown in Figure 7 together with the typical vertical velocity that directs them outward (induces an outward motion). Spatial modes corresponding to the dominant frequencies are reconstructed and plotted at three different time period and phase angles for a specific supply flowrate. The red colour on the 2D map corresponds to high axial velocity (greater than mean velocity), and conversely, the blue colour represents negative axial velocity. For the sake of illustration, actual negative axial velocities vectors are added to the positive average velocity. The onset of the instability occurs at the entrance, slightly on either side of the hole. Overall, the velocity is positive. However, the velocity vectors change sign primarily in the curtain region and downstream. The spatial modes are

some kind of low-frequency oscillation associated with the DMD modes rather than the expected recirculation observed earlier (see Figure 3).



t = 5 ms ($\phi = 60^0$) t = 10 ms ($\phi = 120^0$) t = 20 ms ($\phi = 240^0$)

Figure 7 : DMD Relative spatial axial velocities in the liquid curtain at 18.2 Hz with supply flow rate of Q = 0.18 m^3/mh.

4 Conclusions

For the first time, a new non-intrusive optical technique, 2D 2C optical flow with the concept of defocus was implemented for characterization of liquid film on a "metallic" vertical perforated plate (single perforation). A new type of image processing technique by optical flow algorithm is used to measure 2D velocity of the flow.

Local trajectories were measured in curtain mode ("twin liquid films") on a perforated plate for different supply flow rates. The liquid film recirculation is predominantly observed in the liquid curtain at stagnation points. In other words, impingement of the curtain on the exit edge of the perforation results in a pair of counter rotating vortices ($d = 4\,mm$, kidney-pair vortices). This is an important observation in case of twin liquid films when compared to the wall-bounded liquid films. Vortex structures in the flow are known to transport the liquid phase toward the interface in counter-current flow, producing steeper concentration gradients at the interfaces. As a result, the mass fluxes through the interface increase, and then mass transfer intensifies. The stagnation points may reduce the liquid film velocity locally, increasing the local residence time, leading to a longer gas-liquid contact time.

Finally, DMD analysis is applied to extract the dynamic information of the liquid curtain by the reconstruction of spatial modes corresponding to the dominant frequencies of the flow field. The flow patterns in the liquid curtain resemble low-frequency oscillations type of flow. These oscillations are initiated at the entrance of the perforation. It is observed to develop in the liquid curtain and propagates downstream the perforation.

A rigorous interpretation of the results is however, necessary to confirm their impact in mass transfer intensification in corrugated and perforated structured packing.

Bibliography

1. Schug S. Imaging of Fluid Dynamics in a Structured Packing Using X-ray Computed Tomography. 2016;(8):1561-1569.
2. Fourati M, Roig V, Raynal L. Experimental study of liquid spreading in structured packings. *Chem Eng Sci*. 2012;80:1-15.
3. Gerke SJ, Leuner H, Repke J. Experimental Investigation of Local Film Thickness and Velocity Distribution Inside Falling Liquid Films on Corrugated Structured Packings. 2018;69:1-6.
4. Xie H, Hu J, Wang C, Dai G. Liquid flow transition and confined free film formation on a vertical plate with an open window. *Exp Therm Fluid Sci*. 2018;92(July 2017):174-183.
5. Iyer M, Duval H, Casalinho J, Seiwert J, Wattiau M. Experimental study of a liquid film flowing over a perforation. *AIChE J*. 2021;67(11):e17363.
6. Xie H, Hu J, Dai G. Numerical simulation on flow behavior of twin-liquid films over a vertical plate with an open window. *AIChE J*. 2018;64(4):1458-1468.
7. Baudoin R, Zimmer L, Muller T. Development and application of a time resolved dual camera 3D PTV technique around obstacles using defocus concept downstream a spacer grid. 2014;(July).
8. Sun D, Roth S, Black MJ. A quantitative analysis of current practices in optical flow estimation and the principles behind them. *Int J Comput Vis*. 2014;106(2):115-137.
9. Bruhn A, Weickert J SCL meets H. Combining local and global optic flow methods. *Int J Comput Vis*. 2005;61(3):211–231.